Neural excitatory rebound induced by valproic acid may predict its inadequate control of seizures

Xiang Zou,[b,e,f,1] Zilu Zhu,[a,1] Yu Guo,[b,1] Hongmiao Zhang,[c,1] Yuchen Liu,[a] Zhengyu Cui,[d] Zunji Ke,[d] Shize Jiang,[b,e,f] Yusheng Tong,[b] Zehan Wu,[b,e,f] Ying Mao,[b,e,f,g,h,i*] Liang Chen,[b,e,f,g,h*] and Deheng Wang [a**]

[a]School of Basic Medical Sciences, Shanghai University of Traditional Chinese Medicine, Shanghai 201203, China
[b]Department of Neurosurgery, Huashan Hospital, Fudan University, Shanghai 200040, China
[c]College of Mechanical and Electrical Engineering, Soochow University, Suzhou, 215000, China
[d]Academy of Integrative Medicine, Shanghai University of Traditional Chinese Medicine, Shanghai 201203, China
[e]Neurosurgical Institute of Fudan University, Shanghai 200040, China
[f]Shanghai Clinical Medical Center of Neurosurgery, Shanghai 200040, China
[g]Shanghai Key Laboratory of Brain Function and Restoration and Neural Regeneration, Shanghai 200040, China
[h]Tianqiao and Chrissy Chen International Institute for Brain Diseases, Shanghai 200040, China
[i]State Key Laboratory of Medical Neurobiology and MOE Frontiers Center for Brain Science, School of Basic Medical Sciences and Institutes of Brain Science, Fudan University, Shanghai 200040, China

Summary

Background Valproic acid (VPA) represents one of the most efficient antiseizure medications (ASMs) for both general and focal seizures, but some patients may have inadequate control by VPA monotherapy. In this study, we aimed to verify the hypothesis that excitatory dynamic rebound induced by inhibitory power may contribute to the ineffectiveness of VPA therapy and become a predictor of post-operative inadequate control of seizures.

Methods Awake craniotomy surgeries were performed in 16 patients with intro-operative high-density electrocorticogram (ECoG) recording. The relationship between seizure control and the excitatory rebound was further determined by diagnostic test and univariate analysis. Thereafter, kanic acid (KA)-induced epileptic mouse model was used to confirm that its behavior and neural activity would be controlled by VPA. Finally, a computational simulation model was established to verify the hypothesis.

Findings Inadequate control of seizures by VPA monotherapy and post-operative status epilepticus are closely related to a significant excitatory rebound after VPA injection (rebound electrodes $\geqq 5/64$, $p = 0.008$), together with increased synchronization of the local field potential (LFP). In addition, the neural activity in the model mice showed a significant rebound on spike firing (53/77 units, 68.83%). The LFP increased the power spectral density in multiple wavebands after VPA injection in animal experiments ($p < 0.001$). Computational simulation experiments revealed that inhibitory power-induced excitatory rebound is an intrinsic feature in the neural network.

Interpretation Despite the limitations, we provide evidence that inadequate control of seizures by VPA monotherapy could be associated with neural excitatory rebounds, which were predicted by intraoperative ECoG analysis. Combined with the evidence from computational models and animal experiments, our findings suggested that ineffective ASMs may be because of the excitatory rebound, which is mediated by increased inhibitory power.

Funding This work was supported by National Natural Science Foundation of China (62127810, 81970418), Shanghai Municipal Science and Technology Major Project (2018SHZDZX03) and ZJLab; Science and Technology Commission of Shanghai Municipality (18JC1410403, 19411969000, 19ZR1477700, 20Z11900100); MOE Frontiers Center for Brain Science; Shanghai Key Laboratory of Health Identification and Assessment (21DZ2271000); Shanghai Shenkang (SHDC2020CR3073B).

eBioMedicine 2022;83: 104218
Published online xxx
https://doi.org/10.1016/j.ebiom.2022.104218

*Corresponding authors at: Department of Neurosurgery, Huashan Hospital, Fudan University, No. 12 Wulumuqi Zhong Road, Shanghai 200040, China.
**Corresponding authors at: School of Basic Medical Sciences, Shanghai University of Traditional Chinese Medicine, 1200 Cailun Rd, Shanghai 201203, China.
E-mail addresses: hs_maoying@vip.126.com (Y. Mao), chenlianghs@126.com (L. Chen), wangdeheng@shutcm.edu.cn (D. Wang).

[1] These authors contributed equally to this work.

Keywords: Neural excitation; Rebound; Antiseizures medications; Seizure

Research in context

Evidence before this study

Valproic acid (VPA) represents one of the most classic antiseizure medications (ASMs), but some patients have inadequate control of seizures by VPA monotherapy. For craniotomy, prophylactic use of ASMs such as VPA may sometimes fail to prevent postoperative seizures. There is no reliable factor to predict such inadequate control of seizures.

Added value of this study

By intraoperative high-density electrocorticogram (ECoG) study, we demonstrated neural excitatory rebound induced by VPA is a general phenomenon and closely related to postoperative inadequate control of seizures by VPA monotherapy. Then, *in vivo* study confirmed rebounds on spike firing and the local field potential (LFP) power spectral density in multiple wavebands after VPA injection. Finally, computational simulation experiment revealed excitatory rebound induced by inhibitory power may be an intrinsic feature in neural network.

Implications of all the available evidence

Significant excitatory rebound induced by VPA may become a predictor for its effect. Intraoperative ECoG could be broadly applied to guide postoperative antiseizures regimen, which provides new insight into precision medicine.

Introduction

Epilepsy is a neurological disorder characterized by excessive or hyper-synchronous discharge of neurons because of excitatory/inhibitory imbalance.[1] The inhibitory power is assumed to reduce neuron activity. Therefore, antiseizure medications (ASMs) are designed to have decreasing excitability or increasing inhibitory ability. Valproic acid (VPA) has been introduced into clinical practice over 50 years and has become the first-line drug for several epileptic diseases nowadays.[2] Pre- and post-synaptic effects of VPA rely on a broad action spectrum, including the regulation of ionic currents and the facilitation of inhibitory over excitatory neurotransmitters. One of the main action mechanisms of VPA is the modulation of gamma-aminobutyric acid (GABA)-ergic transmission. Specifically, VPA improves the inhibitory activity of GABA by promoting the availability of synaptic GABA[3] and by enhancing the stimulus-induced responses of both GABA-A and GABA-B receptors.[4] The selective enhancement of GABA-ergic transmission increases brain GABA concentration after VPA treatment.[5] However, VPA monotherapy has limitations including inferior efficacy in seizure control in secondary generalized tonic-clonic seizures, focal impaired awareness seizures, and some status epilepticus.[6] In rare cases, ASMs are reported to aggravate the existing seizures or induce a new seizure type.[7] In addition, VPA-induced seizure aggravation has been reported in some cases for unknown reasons.[8,9] For intracranial lesion surgery, prophylactic use of ASMs is sometimes inefficacious. 20%–40% of brain tumor patients with seizures episodes will develop after treatment. Perioperative ASMs prophylaxis for brain tumor surgery only partially provides reduction in seizure risk.[10] However, there is still no theoretical explanation or predictor for this issue.

Despite the molecular antiepileptic mechanism of VPA, we also need to consider the potential mesoscopic dynamic mechanisms of VPA on neuron populations. Based on our clinical observation, we hypothesized that the inhibitory power from ASMs may have the possibility of inducing membrane potential synchronization and causing oscillation of the local field potential by a network intrinsic dynamic mechanism. We aimed to verify the hypothesis that excitatory dynamic rebound induced by inhibitory power may contribute to the ineffectiveness and become a predictor of post-operative inadequate control of seizures, including focal or generalized type either in early or late stage, as well as the more dangerous status epilepticus. The inadequate control may be associated with neural excitatory rebound together with increased synchronization of the local field potential (LFP), which were revealed by intraoperative electrocorticography (ECoG). A computational model across neuron and population levels on the Hindmarsh–Rose neuron model[11] was established and animal experiments were performed to verify the hypothesis. Based on our results, we propose a relatively universal theory explaining the dichotomous role of inhibitory power.

Methods

Ethics statement

The data collected from human subjects were approved by the Ethics Committee of Huashan Hospital, Fudan

University (approval numbers KY2014-240, KY2015-256, and KY2019-518) and conducted in accordance with the Helsinki Declaration. All patients provided their written informed consent. All experiments in the study involving live animals were approved by the Institutional Animal Care and Use Committee at the Shanghai University of Traditional Chinese Medicine.

Human subjects' data collection

We collected the data from 16 consecutive patients, 11 of whom presented with seizures. As the lesions were related to the eloquent area, all patients underwent awake craniotomy. The inadequate control of seizures is defined as peri-operative focal or generalized type seizures and early post-operative status epilepticus, by routine prophylactic ASMs regimen. Recurrent episodes during follow-up are also considered as inadequate control by current regimen. Five of the seizure's onset patients showed less efficient outcomes with the VPA monotherapy before admission. Six of the 16 patients received an additional oxcarbazepine regimen post-operation owing to inadequate control of seizures. Four of the 6 patients developed status epilepticus within 6 h of the surgery and required midazolam maintenance (i.v) for at least 24 h. At our center, we routinely applied prophylactic ASMs (usually VPA or levetiracetam (LEV), 1000 mg/day) to prevent postoperative seizures, in consideration of the subsequent serious complication.[12] If the patient showed no seizures 2 weeks after surgery, we discontinued this regimen. If seizure control was inadequate, we aim to undertake multiple ASMs for at least 6 months. All the patients finished one-year follow-up before this study. The detailed clinical characters are presented in Table 1 and Supplementary Table 1. During the awake craniotomy, a high-density EGoG grid was placed over the lesion and peri-lesion area (8 × 8 electrode configuration, 5-mm inter-electrode spacing, 1.8−2-mm exposed diameter for each electrode; PMT Corporation, Chanhassen, MN, USA; Beijing Sinovation Medical Technology Corporation, Beijing, China). A 1 × 6-mm strip was placed distant from the galea to serve as reference and ground. We used the Natus Quantum LTM Amplifier System (Natus Medical Incorporated, Oakville, ON, Canada) with a sampling rate of 2048 Hz to acquire the ECoG signals. At this sampling rate, we captured signals from 0 to 878 Hz.

Human subject anesthesia and VPA protocol

We applied an asleep−awake−asleep anesthesia protocol for the awake craniotomy. To sedate the patient, we first administered the intravenous anesthetics using dexmedetomidine (DEX) dose of 0.4−0.6 μg/kg of the body weight (BW), followed by the administration of 0.1−0.2 μg/kg of BW/h of maintenance infusion. Propofol was infused via the target-controlled infusion (TCI) strategy at an effect-site concentration (Ce) of 0.8−1.0 μg/mL along with remifentanil (Ce 0.5 ng/mL). The infusion rate of all 3 anesthetics was progressively increased until the patient reached a deep sedation stage (Observer's Assessment of Alertness/Sedation Scale (OAA/S) score of 0−1, which is a measure of consciousness evaluated by an experienced anesthesiologist). Next, we injected a scalp nerve block agent (0.375% ropivacaine + 0.5% lidocain + 1:400000 epinephrine) before securing the patient's head within a stereotactic Mayfield frame. Then, the neurosurgeon performed the craniotomy when patients were placed under deep sedation, followed by placing an 8 × 8-ECoG grid for monitoring. After completing the ECoG placement, we suspended the infusion of propofol and remifentanil, causing the Ce of propofol to decline; the patients were gradually reversed from their sedation until they reached a moderate sedation stage, that is, an OAA/S score of 2−3. We continuously evaluated the OAA/S score at intervals of 5 min. Once the patient reached an OAA/S score of 5, we considered the patient to be awake, and the patient could also perform free-talk and limbs movements. When the patients were awake, the baseline ECoG signal was recorded for 5 min before VPA injection, which is in order to prevent cortical stimulation induced seizures during awake craniotomy.[13] Subsequently, a dose of 0.8 g sodium valproate (12−18 mg/kg) was intravenously injected within 10 s, and the ECoG signal was recorded for another 5 min.

Human data processing

For the human ECoG signals, time-frequency power spectra analysis was performed as described previously.[14] Then, we calculated the average power during the 5 min before and after VPA injection for each electrode. We then also classified the ECoG frequency spectrum into 3 frequency bands: slow waves (3−5 Hz), sharp waves (6−12 Hz), and spike waves (13−30 Hz) for each electrode, following the clinical classification. The power gradient ratio was calculated as the difference divided by the initial power. The power gradient ratio >1 is considered to be a significant excitatory rebound. Significant excitatory rebound electrodes were summed in each frequency band and for each patient for the following analysis.

In addition, we calculated the difference in the average power and channels' synchronization between the 2 periods. We then selected the channels of shifted power as the interesting pairs (Supplementary Method 1 in detail).

Animal Subjects

Total of 43 male (3-4 month old, purchased from Beijing Vital River Laboratory Animal Technology Co., Ltd.)

Patient	Gender	Age	Symptom	Lesion location	Surgical result	Pathology	Post-operative status epilepticus	Post-operative medications
1	M	42	Seizures	R temporal	GTR	AVM	No	VPA
2	F	42	Seizures	L frontal and insular	STR	Oligodendroglioma WHO II	No	VPA
3	F	29	Seizures	R frontal and temporal	GTR	Anaplastic astrocytoma WHO III	No	LEV
4	F	44	Seizures	L frontal	GTR	Cavernous malformation	Yes	LEV+OCX
5	F	38	Seizures	L frontal	GTR	Astrocytoma WHO II	No	VPA
6	M	41	Seizures	R frontal	STR	Anaplastic astrocytoma WHO III	No	LEV+OCX
7	M	38	Seizures	R frontal and callosum	STR	Oligodendroglioma-Astrocytoma WHO II	No	LEV+OCX
8	M	51	Asymptom	L frontal	GTR	Cavernous malformation	No	VPA
9	M	47	Asymptom	R frontal	GTR	Anaplastic astrocytoma WHO III	No	VPA
10	M	28	Seizures	L frontal	GTR	Foam cells with hemosiderin deposition	Yes	LEV+OCX
11	F	41	Headache	L temporal	GTR	Astrocytoma WHO II	No	LEV
12	M	36	Seizures	L temporal	GTR	Astrocytoma WHO II	No	LEV
13	F	39	Hemiplegia	L frontal	STR	Glosis	Yes	LEV+OCX
14	F	18	Seizures	R frontal	GTR	Dysembryoplastic neuroepithelial tumor	Yes	LEV+OCX
15	F	41	Seizures	R frontal	GTR	Anaplastic Oligodendroglioma WHO III	No	LEV
16	F	25	Dizziness	L frontal	GTR	Oligodendroglioma WHO II	No	VPA

***Table 1*: Baseline characteristics of the patients.**
VPA = valproic acid; LEV = levetiracetam; OXC = oxcarbazepine; GTR = gross total resection; STR = sub-total resection.

C57BL/6J mice were used in animal behavior tests and in *vivo* recording experiments. Animals were housed at our university animal facility (housed separately with the headstage implant) with a 12-h light-dark cycle at a constant temperature (24 ± 1°C) and humidity (50 ± 5%) and supplied with food and water *ad libitum*. All experiments were conducted during the light cycle and the protocol was prepared before the study. Littermates were randomly assigned to each group by the operator, using the standard = RAND () in Microsoft Excel. The animal behavior and in *vivo* recording experimenters were blinded to the group allocation of the mice. All animal procedures were approved by the Shanghai University of Traditional Chinese Medicine Institutional Animal Care and Use Committee.

KA Induced Epilepsy Animal Models and antiepileptic animal models

We employed two different doses (10 mg/kg low dose[15] and 30 mg/kg high dose,[16] 12 animals for each group) of KA to induce epilepsy (intraperitoneal injection, i.p.) in separate animal groups. The low-dose animal group was selected owing to the low rate of animal mortality (mortality rate: 10 mg/kg group: 0/12; 30 mg/kg group: 9/12 mice, since we were not able to calculate the effect size and the relative power value of these two groups, we used the resource equation approach to calculate the sample size: E = (12 + 12) − 2 = 22 > 10, we consider the sample size to be sufficient.[17]). An hour-long behavior monitoring was performed to observe seizure conditions immediately after the KA i.p. injection. The epilepsy-like behavior included wet-dog shaking, forelimb clonus, or tonic-clonic convulsions.[18] All behavior data were presented as mean ±SEM. Differences were considered to be significant at $p < 0.05$. As for the antiepileptic model, the mice were administered with VPA 2 min after the KA injection; the VPA was injected a total of 5 times at 70 mg/kg body weight every 2 min, followed by a 35 mg/kg of dose every 5 min until the epilepsy behavior disappeared (totaling 1 h). For the VPA treatment, we used continuous i.p. injection of a low dose to alleviate the possible side-effects of VPA and reduce animal mortality.[19,20]

Animal surgery and *in vivo* recording of neural activity

Electrophysiology data were obtained from the hippocampal CA1 brain region of freely behaving mice with implantation of 32-channel recording arrays. Total 21 mice were employed in vivo recording experiments, the animal sample size was decided by the number of neuronal spikes recorded (> 50 spikes total; > 10 spikes per animal), no criteria were set for including or excluding animals and no mice were excluded in this study.[21] The recording electrodes consisted of movable bundles of tetrodes that were constructed by twisting 4 fine wires (California Fine Wire #100-167). The animals were handled for a minimum of 3 days before the electrode implantation surgery. After several days of animal handling, the animals were anesthetized with an i.p. injection of 100 mg/kg pentobarbital sodium. The electrode tips were positioned in the specific brain region above the hippocampal CA1 (AP -2.3 mm, ML 2 mm, DV 1 mm). To eliminate the possible effects of barbiturates on the neural activity and to allow for sufficient recovery time, the mice were placed in a home cage for at least 1 week before conducting the neural recording (5-8 mice for each group, based on the number of units recorded).

We recorded the neuronal activity from the hippocampal CA1 region in free behaving mice. These mice were assigned to three in *vivo* recording groups (7 mice each): KA-induced Epilepsy Animal Model, KA+ VPA antiepileptic animal model and VPA control group. For the KA and KA+VPA groups, the modeling methods are mentioned before. And for the VPA control group, the mice were provided the antiepileptic drug VPA at 70 mg/kg body weight dosage every 2 min, totaling 5 times (total time taken 10 min) after 30 min of free exploration in the home cage. Then, the animals were simultaneously observed for their behavior and neural activity. Briefly, the electrode was slowly advanced to the destination region (proximately 35 μm/day). After the *in vivo* recording, the mice were anesthetized and a certain amount of current was delivered to the electrode tip in order to mark the position of the electrode tip. Then, their position was confirmed by histological staining (Nissl, 0.1% cresyl violet) of the brain tissue slice.

Animal data collection and processing

The single-unit spike and local field potential from the experimental mice were simultaneously recorded by the OmniPlex Neural Data Acquisition System (Plexon Inc., Dallas, TX). Spikes that showed adjustable online thresholds were collected at 40 kHz. Then, these spikes were sorted and identified by the Offline Sorter 4.0 software and Matlab program (KlustaKwik 1.7 and MClust 3.5: http://redishlab.neuroscience.umn.edu/MClust/MClust.html). Peri-event histograms, correlation with LFP, and coherence of LFP and power spectral density (PSD) were conducted in the NeuroExplorer 5 (Nex Technologies). All smoothing with histograms was conducted by using the Gaussian filter (filter width = 3 bins).

Characterization of neuronal responses

To determine whether a recorded unit was responsive to drug injection, we employed the i.p. injection time point as time zero to calculate a peri-event histogram using a 30-s bin size. The neuronal activities 10 min before the i.p. injection served as the baseline to determine the confidence interval. To evaluate the presence of any

significant changes in the firing frequency, we first defined 80% confidence intervals as a threshold to detect any significant response (firing rate increase or decrease within a certain duration after drug injection). Then, if the change in the firing rate reached 95%, 99.9%, 99.999%, and 99.99999% confident intervals, and the duration was >5 bins, 3 bins, and 2 bins, respectively.[22] We considered this unit to indicate a significant neuronal response (increased or decreased).

Simulation experiments

To determine the dynamic features of the neural excitatory rebound induced by inhibitory power, we conducted computational simulation experiments based on the Hindmarsh-Rose model. In this neural cluster, we adjust the inhibitory power including the proportion and synapse weight, then calculate the synchronization factor of membrane potential among excitatory neurons. Details are described in Supplementary file - Method 2.

Statistical Analysis

Unless indicated otherwise, all results are presented as the mean standard error of the mean. The data distribution was examined by Shapiro-Wilk test. Statistical analysis was performed using the Wilcoxon rank-sum test for nonparametric data (applied in clinical data as a result). Variance ratio was determined by F test. Comparison in animal experiments were determined by Student's t test for two groups and one-way ANOVA with the Bonferroni test for post-hoc analysis for multiple groups. Diagnostic accuracies to determine the amount of significant excitatory rebound electrodes were assessed using the area under the receiver-operating characteristic (ROC) curve (AUC). The cutoff, sensitivity, and specificity were determined via the ROC analysis and Youden index. Differences in the clinical features between mono/duotherapy as well as the no/post-operative status epilepticus groups were assessed using Fisher's exact test. Differences in the animal data were analyzed using Two-tailed paired t test, Two-tailed unpaired t test, Ordinary one-way ANOVA and Repeated measures One-way ANOVA. The differences were considered significant for p values < 0.05. All data were analyzed using the SPSS (version 18.0; IBM Corp., Armonk, New York, USA) and the GraphPad Prism 9 software (GraphPad Inc. San Diego, CA, USA).

Role of funding source

The funding sources did not have a role in the study design, data collection, data analysis, interpretation, or writing of report.

Results

Excitatory rebound is a common phenomenon of VPA treatment in human subjects

All 16 patients completed their awake procedures successfully with no intro-operative complications. To investigate the ECoG frequency spectrum power shift by VPA treatment, we analyzed ECoG data from all the human subjects. The typical intraoperative procedure is shown in Figure 1a, and ECoG signals are shown in Figure 1b before and after VPA injection. We classified the ECoG frequency spectrum into three frequency bands: slow waves (3–5 Hz), sharp waves (6–12 Hz), and spike waves (13–30 Hz) for each electrode. The average spectrum power shift of the three bands with VPA injection in three typical patients is shown in Figure 1c as examples. We found that all the 16 patients had excitatory rebounds by VPA treatment, presented as the increased spectrum power gradient ratio in at least one electrode. Interestingly, in some excitatory rebound electrodes, the increased lower frequency spectrum power transferred from higher to lower frequency bands in situ electrodes after VPA injection (Figure 1d,e). To further confirm the synchronization of these waves after VPA treatment, we selected brown channels in spike wavebands, green channels in sharp wavebands, and purple channels in slow wavebands to calculate the phase-locking value of these channels. All three wavebands showed a significant increase after VPA injection, indicating that VPA could enhance the synchronization of brain waves (Figure 1f-h).

Predictive value of significant excitatory rebound induced by VPA

We determined the predictive amount of significant excitatory rebound electrodes. By performing ROC analysis, the AUC for duotherapy was found to be 0.87 ($p = 0.017$, Figure 2a), with the cutoff value of 5 (sensitivity% = 83.33 and specificity% = 90.00). For status epilepticus, the AUC was 1.00 ($p = 0.0036$, Figure 2b), with the cutoff value of 9 (sensitivity% = 100.00 and specificity% = 100.00). In 6 of the 16 patients, intraoperative ECOG showed a wide significant excitatory rebound (more than 5 electrodes) induced by VPA in any of the three frequency bands. Notably, 5 in those 6 patients required administration of oxcarbazepine regimen for seizure control after surgery (OR = 45, CI: 2.287–885.601, $p = 0.008$). Moreover, 4 in the 6 patients developed status epilepticus within 6 h after surgery and required midazolam administration for maintenance of seizure control for at least 24 h ($p = 0.008$). Among the 10 fewer-rebound patients, 9 became seizure-free by VPA monotherapy (some changed to LEV for hepatic impairment concern). Considering other possible related clinical characteristics such as onset symptoms, lesion location, and extent

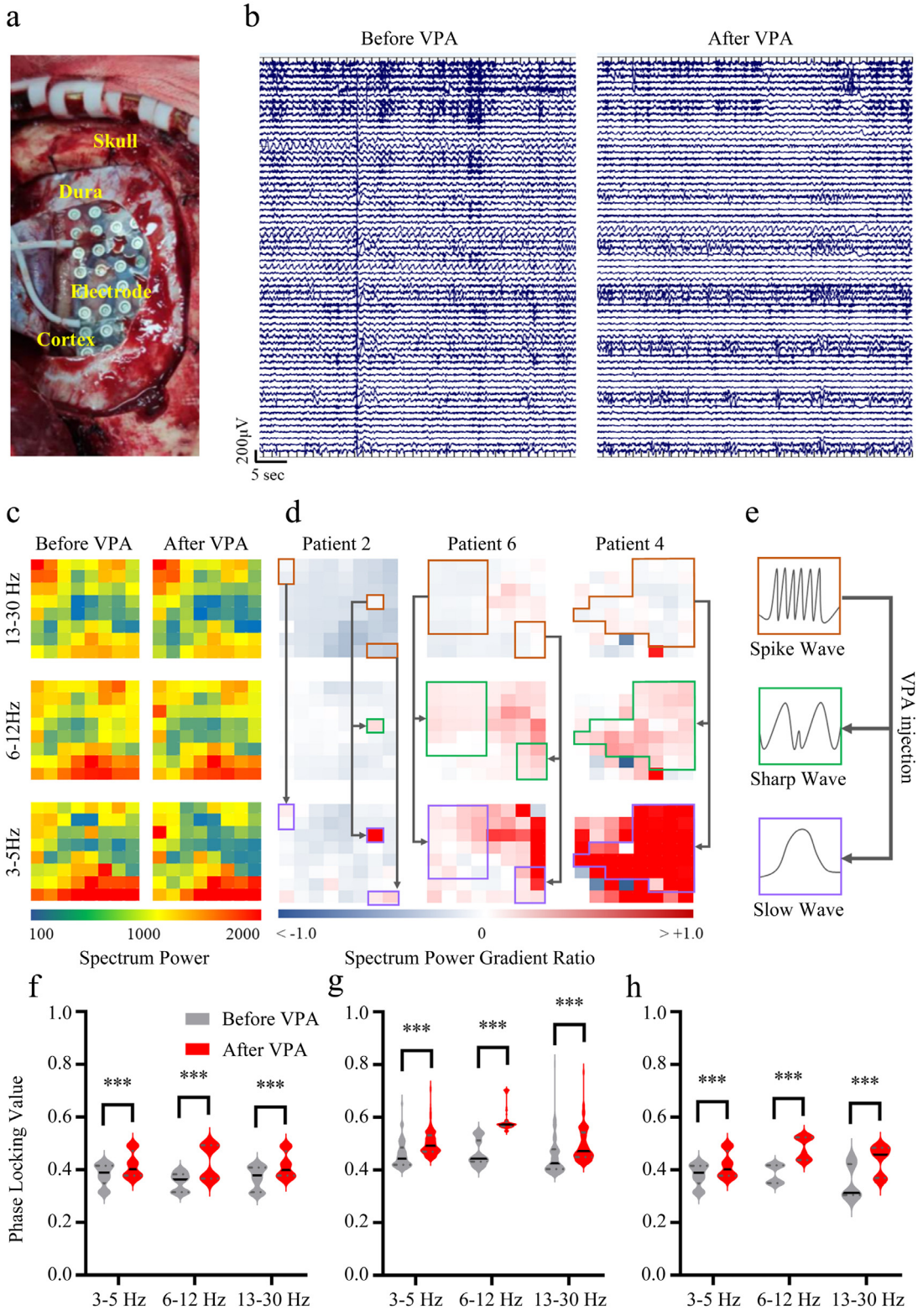

Figure 1. Frequency spectrum power analysis for ECoG signals. (a) Intra-operation electrode implantation. **(b)** Typical ECoG signals before and after VPA injection during five minutes. **(c)** Average frequency spectrum power of slow waves (3-5 Hz), sharp waves (6-12 Hz) and spike waves (13-30 Hz) for each electrode, before and after VPA injection during five minutes. **(d)** Spectrum power

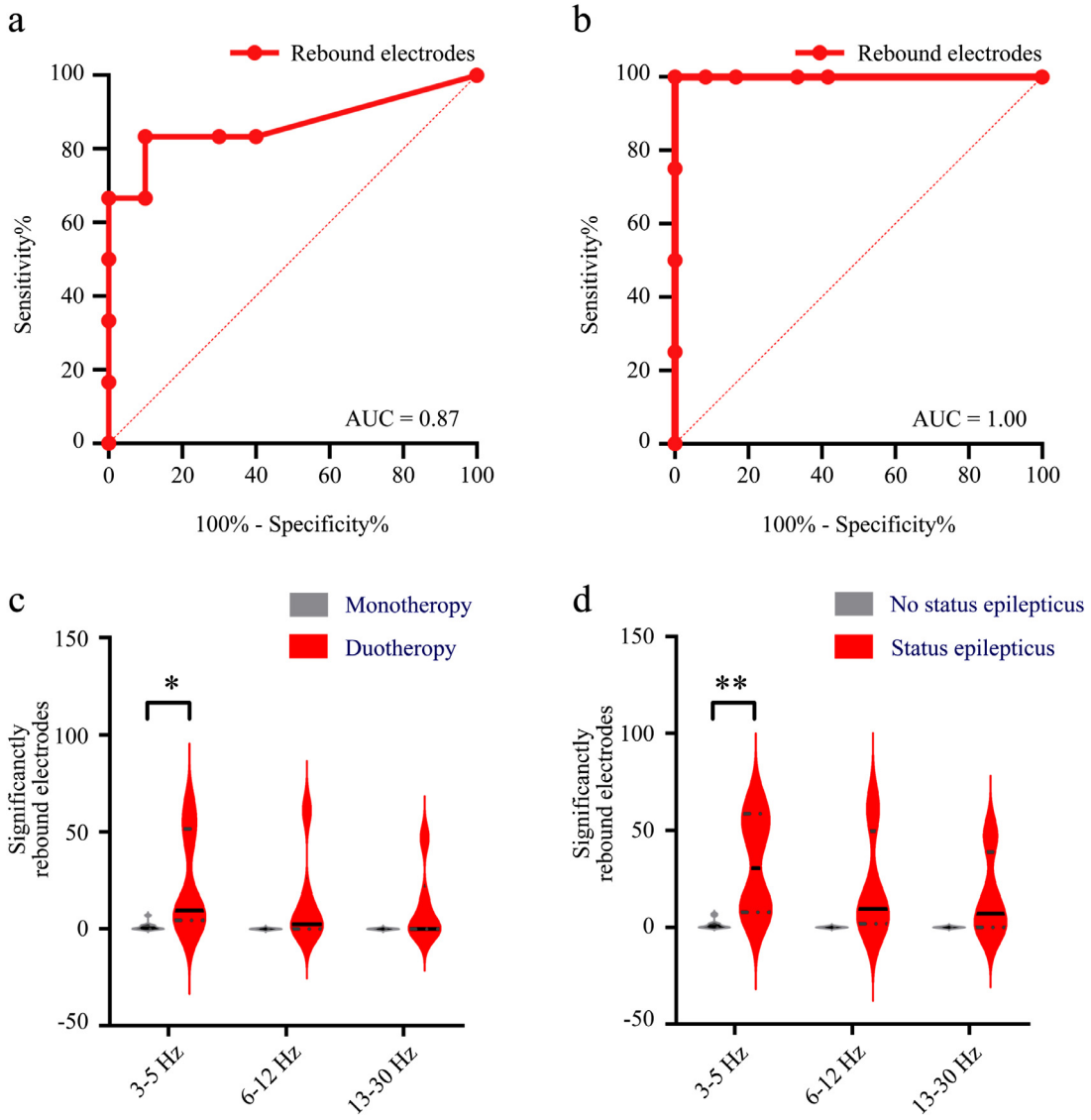

Figure 2. Inadequate control of seizures by VPA is correlated with significant excitatory rebound. (a) ROC analyses for distinguishing monotherapy and duotherapy subjects ($n = 16$); (b) ROC analyses for distinguishing status epilepticus and no status epilepticus subjects ($n = 16$); (c) Comparison of rebound electrodes amounts between monotherapy and duotherapy group, in three different frequency bands. *$p < 0.05$, Wilcoxon rank-sum test. (d) Comparison of rebound electrodes amounts between status epilepticus and no status epilepticus group, in three different frequency bands. **$p < 0.01$, Wilcoxon rank-sum test. Sensitivity and specificity were calculated using the cutoff that produced the highest Youden index (sensitivity + specificity −1). AUC = Area under the receiver-operating characteristic (ROC) curve.

of resection, none of the patients had significant correlations with VPA ineffectiveness. The details are given in Table 2. In addition, the number of significant rebound electrodes in the duotherapy group was remarkably larger than in the monotherapy group for the 3–5 Hz band (22.50 ± 10.57 vs. 1.30 ± 0.68, $p = 0.0128$, Figure 2c). Similarly, the number of significant rebound electrodes in the status epilepticus group was much larger than in the no status epilepticus group (32.25 ± 13.52 vs. 1.58 ± 0.70, $p = 0.003$, Figure 2d). Notably, 10

gradient ratio before and after VPA injection. Brown regions: inhibited spike waves; green regions: increased sharp waves in situ; purple regions: increased slow waves in situ. **(e)** Schematic diagram of spike waves shift to sharp waves and slow waves after VPA injection. **(f-h)** Phase locking value of electrodes of brown, green and purple regions, ***$p < 0.001$, Wilcoxon rank-sum test (left: patient 2; middle: patient 6; right: patient 4).

	Antiepileptic regimen			Status epilepticus		
	Monotherapy (n = 10)	Duotherapy (n = 6)	p value	No (n = 12)	Yes (n = 4)	p value
Age	39.2±2.4	34.7±4.0	*0.321*	39.3±2.0	32.3±5.8	*0.163*
Female ratio, %	40%	50%	*1.000*	50%	75%	*0.585*
Initial symptom, n (%)			*0.588*			*1.000*
Seizures attack	6 (37.5)	5 (31.25)		8 (50)	3 (18.75)	
No seizures	4 (25)	1 (6.25)		4 (25)	1 (6.25)	
Hemisphere, n (%)						*0.585*
Left	6 (37.5)	3 (18.75)	*1.000*	6 (37.5)	3 (18.75)	
Right	4 (25)	3 (18.75)		6 (37.5)	1 (6.25)	
Location, n (%)			*0.234*			*0.516*
Frontal	6 (37.5)	6 (37.5)		8 (50)	4 (25)	
Temporal	4 (25)	0 (0)		4 (25)	0 (0)	
EOR, n (%)			*0.118*			*1.000*
GTR	9 (56.25)	3 (18.75)		9 (56.25)	3 (18.75)	
STR	1 (6.25)	3 (18.75)		3 (18.75)	1 (6.25)	
Significant rebound electrodes ≥5, n (%)			*0.008*			*0.008*
Yes	1 (6.25)	5 (31.25)		2 (12.5)	4 (25)	
No	9 (56.25)	1 (6.25)		10 (62.5)	0 (0)	

***Table 2*: Univariate analysis for post-operative antiepileptic regimen and status epilepticus.**
EOR: extent of resection, GTR: gross total resection, STR: sub-total resection.

in 11 patients with post-operative seizures episodes achieved Engel class I at one-year follow-up (Supplementary Table 1).

Seizures induced by KA were significantly suppressed by VPA in mice

We used the mice with kanic acid (KA)-induced epileptic model to test the hypothesis that the behavior and neural activity of animals would be altered by VPA. A bolus dose of KA with an i.p. injection was used to create the models of generalized seizures. The animals were randomly divided into two groups, in which one was injected with KA and the other was injected with KA and VPA (two minutes gap) (Figure 3a). Each group includes 5 mice without headstage implant and 7 mice with headstage implant. The latency of the first epileptic seizure after KA injection and the duration of each epileptic attack was recorded. The latency of the first epileptic seizure of KA-induced epilepsy mice was 48.8 ± 13.25 s and that of the KA + VPA treatment group was 69.6 ± 13.34 s. Both the groups of animals showed seizures in around 60 s ahead of the VPA delivered. No significant difference was found in the seizure latency between the KA modeling mice and the KA + VPA treatment group (ns $p = 0.301$) (Figure 3e). The sham group injected with saline instead of KA and VPA did not show any sign of seizure (data not shown). By using Racine Scale, we calculated the seizure stage for every 2 min in the first hour of KA injection. The average stage of VPA treatment was lowered compared with that of the untreated group (Figure 3b). Compared with the KA group, the VPA treatment group showed significant suppression during the first 15 min (Figure 3c left, $***p < 0.001$), 16–45 min (Figure 3c middle, $***p < 0.001$), and 16–45 min (Figure 3c right, $****p < 0.0001$). The number of seizures in the KA + VPA treatment group within an hour after KA injection was 60.75 ± 18.47, which was significantly lower than that in the KA injection group (167.6 ± 28.47, $*p < 0.05$) (Figure 3d). The duration of each seizure in KA mice was 168.8 ± 38.02 s and that in the KA + VPA treatment group was 39.75 ± 6.498 s. The duration of seizures in the KA + VPA treatment group was significantly lowered (Figure 3f, $*p < 0.05$).

The neural firing was suppressed with VPA injection

We used 64 or 32 channel-tetrode microarrays to record the neuronal spike activity of the hippocampal CA1 brain region while the mice could freely move in their cages (Figure 4a.top). Several neurons can be monitored simultaneously from one tetrode with 7 clusters and waveforms recorded from hippocampal CA1 isolated using the Offline sorting software (Figure 4a.bottom). We implanted electrodes in 7 mice and recorded 139 well-isolated neurons in the hippocampal CA1 region. The majority of neurons in the CA1 brain region in the VPA injection group only showed two different inhibited neuronal spike firing patterns: persistent inhibition until a plateau (50 units 35.97%, Figure 4b left and Figure 4c) and inhibition with firing rebound (82 units 58.99%,

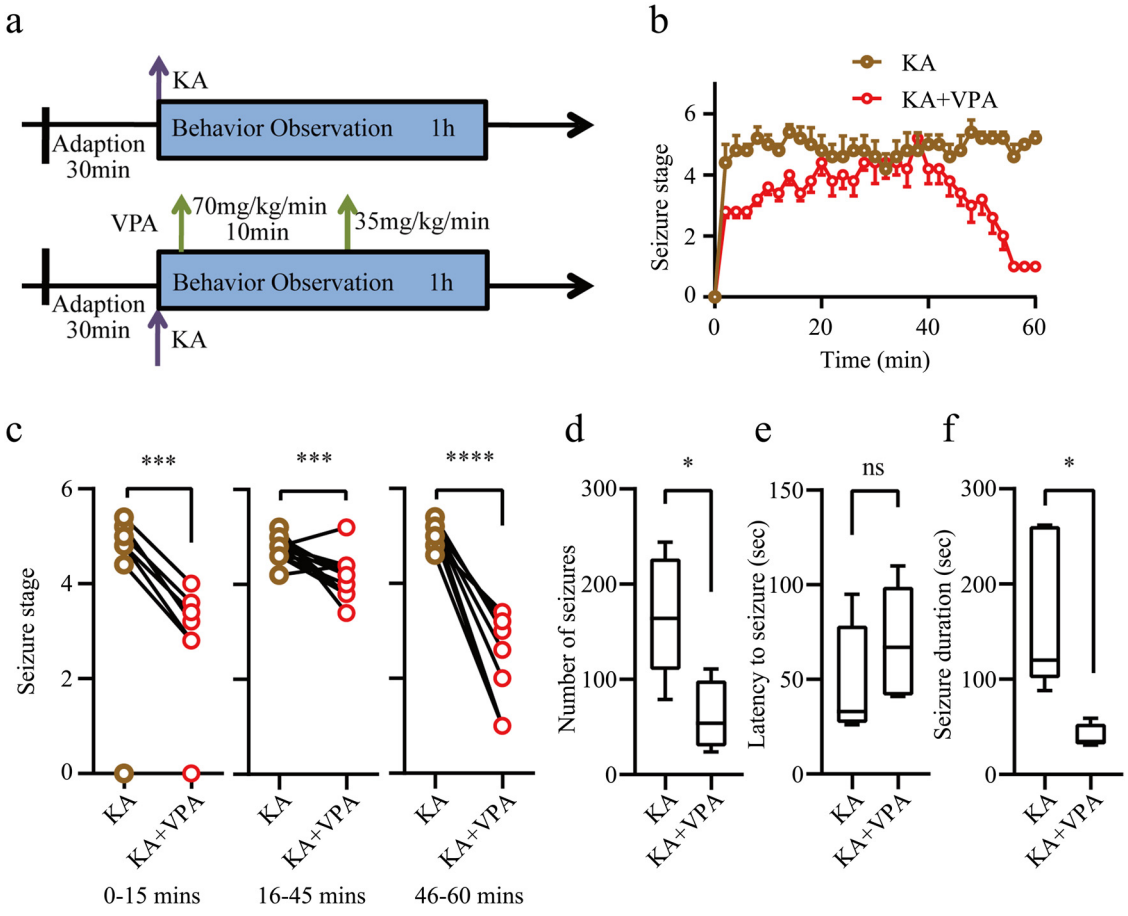

Figure 3. Evaluation of epilepsy behavior in mice. (a) Schematic of KA-inducing seizure and KA-inducing with VPA treatment group. **(b)** The seizure stage of KA and KA+VPA groups based on Racine scale. The Racine scale was estimated in every two minutes. **(c)** The seizure stages of KA and KA + VPA group during the first 15 minutes after KA injection (left). The seizure stages of KA and KA + VPA group during the 16-45 minutes after KA injection (middle). The seizure stage of KA and KA + VPA group during the 46-60 minutes after KA injection (right) (Two-tailed paired *t* test ***$p < 0.001$, ****$p < 0.0001$). **(d)** The number of seizures during 60 minutes after KA delivered ($n = 5$ for each group). Data are presented as mean ±SEM (Two-tailed unpaired *t* test *$p < 0.05$). **(e)** The latency to epileptic seizure. The first seizure discovered after KA injection between 28 to 110 seconds in KA and KA+VPA groups. No seizure was found in VPA group (data did not show) (Two-tailed unpaired *t* test, $p > 0.05$). **(f)** The duration of epileptic seizure (Two-tailed unpaired *t* test *$p < 0.05$).

Figure 4b right and Figure 4c). The rest of the units did not show any firing change after VPA injection (7 units 5.04%, Figure 4c). Furthermore, we compared the units showing spike rebound with the units of decreased firing or no change in correlation with LFP before or after VPA delivery. No significant difference was found between these three groups of units (Figure 4d left and right). Thereafter, we divided the LFP into three different frequency bands (slow wave: 3–5 Hz, sharp wave: 6–12 Hz, and spike wave: 13–30 Hz) and calculated the coherence of LFP. All the three bands of LFP showed that the coherence was significantly lowered after VPA injection (Figure 4e, **$p < 0.01$, ****$p < 0.0001$).

The diversity response of neuronal spike activity and LFP in KA injected mice

We recorded 81 units in 7 mice in the hippocampal CA1 brain region. As expected, the majority of units in the CA1 region showed a significant response to KA injection in terms of inhibition and excitation (Figure 5a and 5c). A total of 77.22% of the responsive units belonged to type 2 excitation and the others belonged to type 1 inhibition (Figure 5c). Moreover, we found that the LFP was changed to high amplitude and high frequency after KA injection (Figure 5b top and bottom). To determine the effect of KA on LFP activity, we calculated the power spectral density and coherence of slow-wave, sharp-wave, and spike-wave bands. PSD in the slow

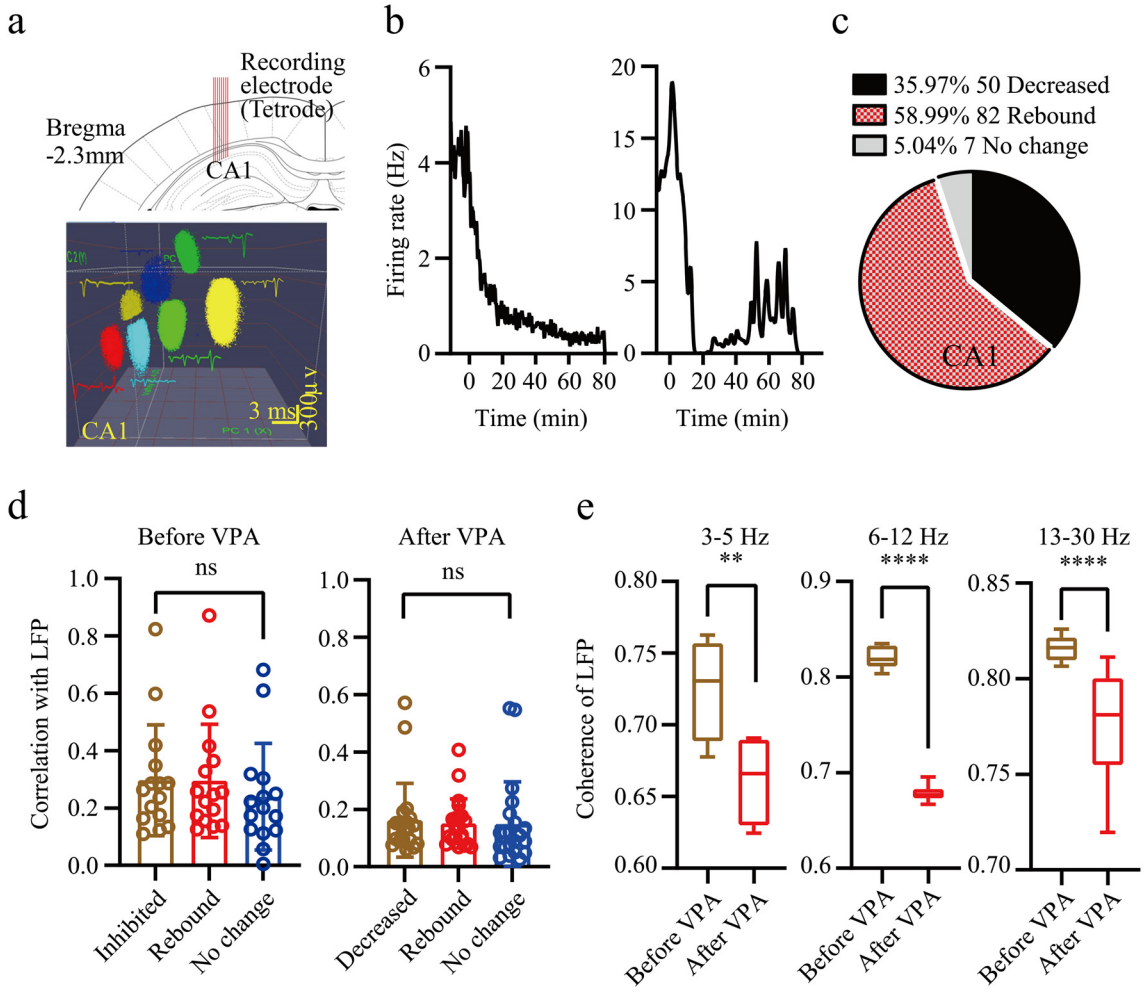

Figure 4. The VPA inhibits the neuron' firing in hippocampal CA1 area. (a) Schematic of tetrode tracks in the mouse hippocampal CA1 brain region (upper), Representative seven well-isolated units (cluster and waveforms) in the PCA plot recorded from the same tetrode in hippocampal CA1 (lower, Scale bar: 3 ms and 300 μv). **(b)** Representative two units from *in-vivo* recording exhibited diversity response to the VPA injection. Peri-event spike histogram show two different responsive units which was an total inhibition (left) and suppressing with an excitation rebound (right). The time zero indicates the time of VPA i.p. injection. **(c)** The ratio of neural activity decreased, rebound and no change units in CA1 brain region. **(d)** The correlation of decreased, rebound and no change units' spikes with the LFP before and after the VPA injection (Ordinary one-way ANOVA, ns $p > 0.05$). **(e)** The coherence of the LFP before and after the VPA injection displayed in different frequency range (3-5 Hz, 6-12 Hz and 13-30 Hz, Two-tailed paired *t* test, $^{**}p < 0.01$, $^{****}p < 0.0001$).

waveband (3−5 Hz) was significantly increased ($^{***}p < 0.001$), whereas that in the sharp waveband (6−12 Hz) increased to the same extent after KA injection ($^{*}p < 0.05$). However, PSD in the spike waveband (13−30 Hz) was reduced significantly (Figure 5d, $^{****}p < 0.0001$). Furthermore, the data on coherence showed that between the slow wavebands, KA increased the coherence of LFPs but reduced the coherence between spike wavebands, and no significant difference was found in the sharp waveband (Figure 5e left to right).

The neuronal spike activity exhibited rebound excitation after VPA inhibition

After we obtained the neuronal activity results of KA-inducing epilepsy or VPA inhibition of epilepsy, we further investigated whether VPA could affect the KA-inducing epilepsy. We recorded 77 units from 7 animals in the hippocampal CA1 brain region. Multiple spike firing patterns were observed from the different brain regions in KA-injected mice after VPA treatment. We separated the units recorded from the CA1 region based on whether the spike neural activity has a rebound

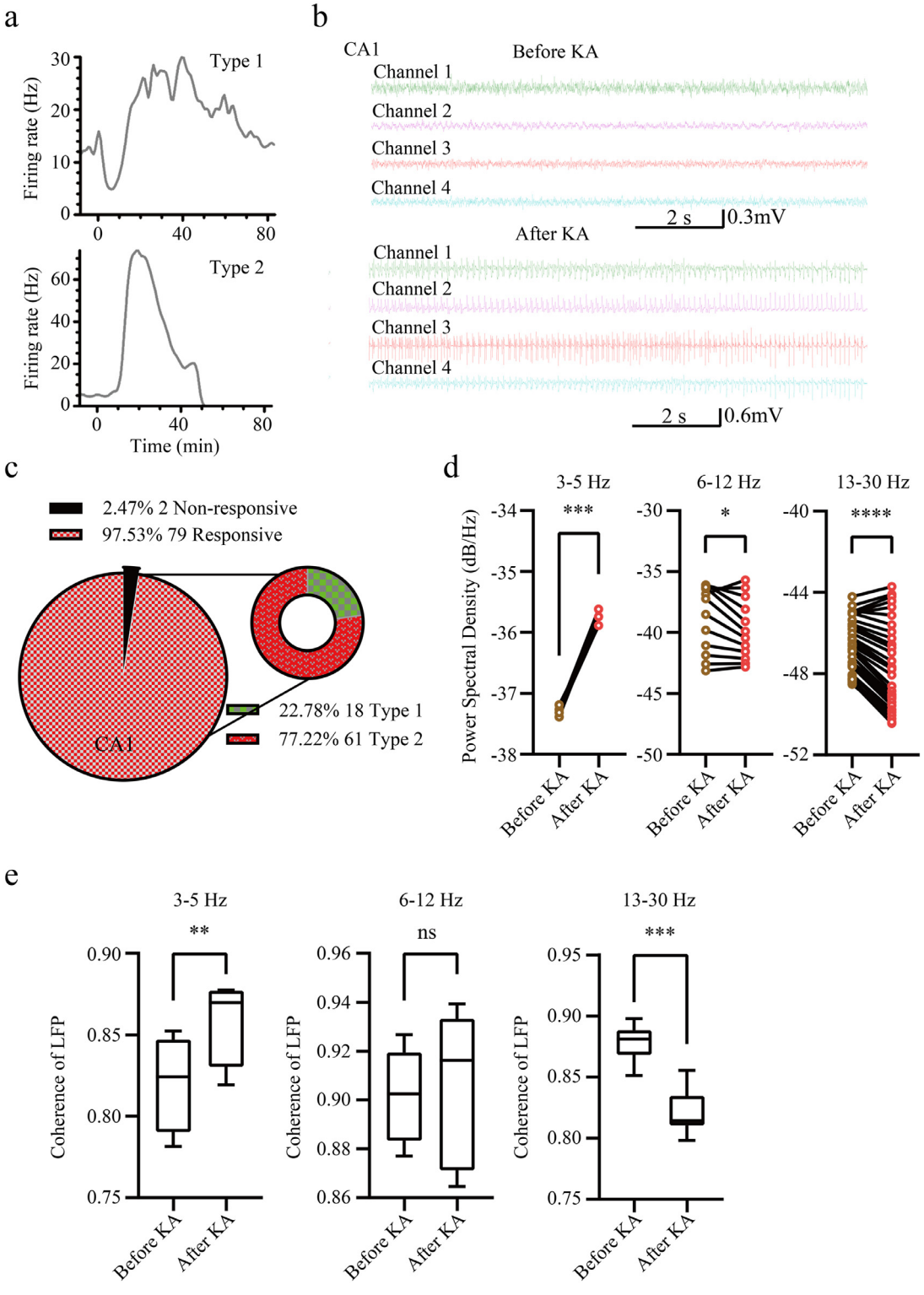

Figure 5. KA-inducing significant increases slow wave band power and reduce spike wave band power in hippocampal CA1. **(a)** Representative units in KA-inducing epileptic animal model. Peri-event spike histogram show two types of responsive units (type 1 and type 2). The time zero indicates the KA i.p. injection. **(b)** Representative LFP traces recorded at different time points before and after KA injection (top: baseline before giving KA, Scale bar: 2 s and 0.3 mV; bottom: after giving KA, Scale bar: 2 s and 0.6 mV). **(c)** The ratio of neural activity show responsive and non-responsive units in CA1 brain region of KA-inducing mice. The

phenomenon (increasing peak firing after decreasing) (Figure 6a left and middle). Certain percentages of units exhibited rebound excitation from a few minutes to over 100 minutes after VPA injection. For instance, 53 units 68.83% of CA1 exhibited rebound excitation after VPA injection (Figure 6b). Among these rebound excitation units, we discovered two different firing patterns based on the neural firing properties. The type 1 pattern was first increased after the drug was delivered and then showed a peak rebound (21 units 39.62% of total rebound units, Figure 6b). The type 2 pattern was decreasing at the beginning and then showed a significant rebound excitation (32 units 60.38% of total rebound units, Figure 6b). Despite these two rebound firing patterns, we discovered the other two patterns with a non-rebound phenomenon. These non-rebound neurons included the units with only one peak of increasing KA-induced firing rate and the non-responsive units (type 3 and type 4). Type 3 showed an increasing firing pattern immediately after KA injection, which is similar to the KA-inducing group (17 units 22.08% of CA1) (Figure 6a,b, Figure 5a). As the rest units did not show a significant response to drug injection, we classified these units as type 4 non-responsive units (7 units 9.09%). For instance, we picked a representative unit of rebound excitation and marked this firing change into 4 stages based on the computational model (Figure 7c). The correlation of four stages with LFP showed a significant difference between S1 and S2 or S4; S3 and S2 or S4, but no significant difference between S1 and S3 (Figure 6c bottom). The results showed that rebound excitation correlates with the correlation between spikes and LFPs. To determine the effect of VPA on LFP of the KA-induced epilepsy model, PSD analysis was performed for different periods including baseline (no drug injection), after KA-inducing, and after VPA. The PSD value after VPA in three wavebands increased significantly (Figure 6e, *** $p < 0.001$). In addition, we performed a coherence analysis to calculate these three wavebands' coherence of LFP, and the results showed that between the slow wavebands, the coherence of LFPs would increase but reduce for the spike wavebands and no statistic significant was found in sharp wavebands (Figure 6f, *$p < 0.05$, ****$p < 0.0001$). These findings suggested that the power and coherence change caused by VPA injection may explain the phenomenon of rebound excitation.

Membrane potential synchronization for excitatory neurons in the neuron cluster with an increasing inhibitory power

The hypothesis that VPA was ineffective because of an excitatory dynamic rebound during an increase in inhibitory power was further verified using a computational model. In the simulation study, we built a cluster consisting of 800 neurons using the Hindmarsh−Rose model, which is described in Supplementary Materials. Generally, this neuron cluster is universal with variable excitatory/inhibitory neuron proportions, random connections, and variable synapse weights. For each variable situation, we calculated the synchronization factor of membrane potential from the excitatory neurons to represent the entire output projection from the cluster. We adjusted the excitatory/inhibitory neuron proportions from 0.50 to 1.20 (0.02 interval), and normalization inhibitory weight from -1.0 to 0.0 (Gaussian distribution, $\sigma^2 = 0.25$, 0.01 interval). For calculating the average synchronization factor on each variable combination, the connections were randomly set to hundred times for calculation. Finally, we obtained a detailed 3-dimensional topography of the synchronization factor by each variable combination (Figure 7a). Interestingly, the synchronization factor will demonstrate a rebound trend with an increase in inhibitory power. In the rebound band, the standard deviation of the synchronization factor will also be increased. Figure 7b shows some typical rebound curves in fixed excitatory/inhibitory proportions. Representative LFPs and spikes on the synchronization factor curve are shown in Figure 7c, demonstrating the four stages under the increasing inhibitory power. The spike patterns have a high frequency by higher excitatory power in stage 1. When the inhibitory power was increased, some neurons' spikes were inhibited in stage 2. In stage 3, the spike frequency became lower but was with more synchronized discharge, thus resulting in recurrent higher LFP oscillation.

Discussion

In this study, 11 in 16 patients presented with seizures, which highlights the need for a predictive marker for postoperative ASMs regimen. The need for prophylactic ASMs remains controversial and lacks of convincing evidence, especially for eloquent brain tumor under awake craniotomy. Report from American Academy of Neurology (AAN) suggested "in patients with brain

percentage of type 1 or 2 of the responsive units at the right panel. **(d)** The power spectral density of different frequency range during baseline recording, after KA injection (left: 3-5 Hz, middle: 6-12 Hz, right: 13-30 Hz, Two-tailed paired *t* test, *$p < 0.05$, ***$p < 0.001$, ****$p < 0.0001$). **(e)** The coherence of the LFP before and after the KA injection displayed in different frequency range (left: 3-5 Hz, middle: 6-12 Hz, right: 13-30 Hz, Two-tailed paired *t* test, **$p < 0.01$, ***$p < 0.001$).

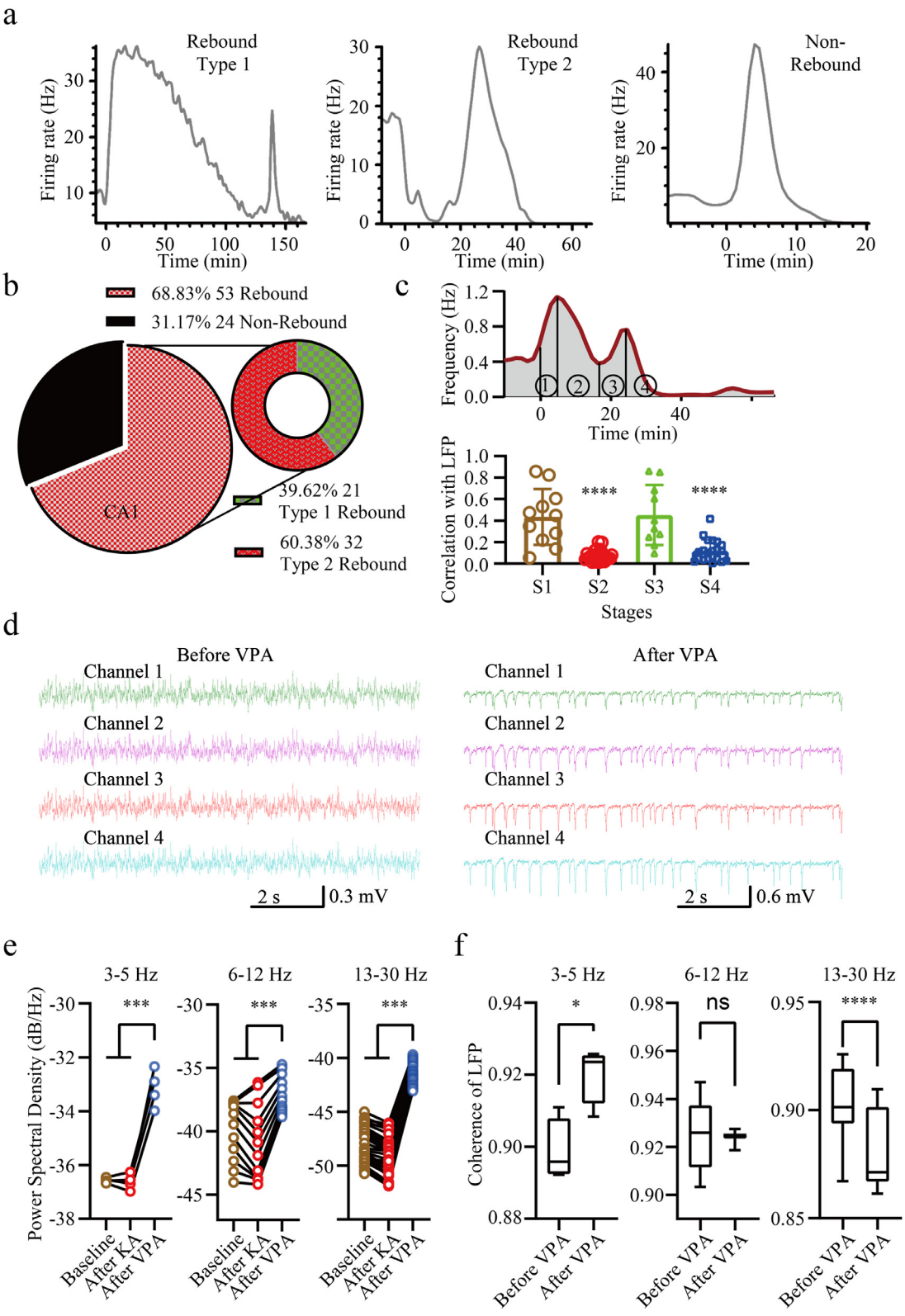

Figure 6. The neuronal activity exhibited rebound excitation after VPA inhibition. (a) Representative units from in-vivo recording exhibited diversity response to the KA injection and VPA treatment. The blue dash line indicates the KA i.p. injection. Peri-event

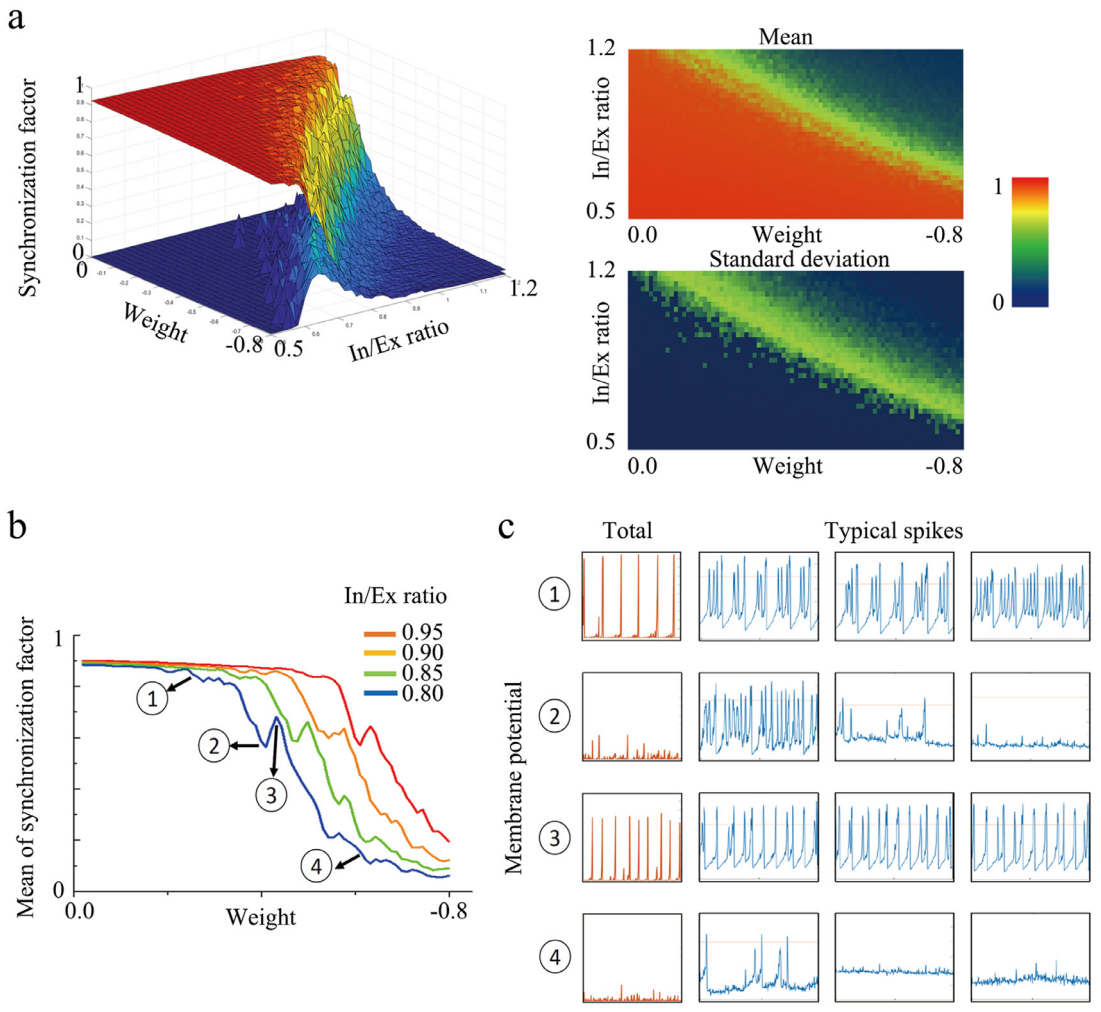

Figure 7. Membrane potential synchronization for excitatory neurons in the neuron cluster with the increasing inhibitory efficiency. (a) The value of synchronization factor of membrane potential for excitatory neurons in the neuron cluster, with gradual increasing inhibitory weight and inhibitory neuron distribution. The upper layer in the 3D and the upper panel in the 2D illustration are the mean values, while the lower layer and panel are the standard deviations. The total neuron amount in the cluster is 800, the inhibitory/excitatory ratio varies from 0.5 to 1.2, step 0.02. The mean weight of excitatory synapses is 0.5 (SD = 0.5); while the mean weight of inhibitory synapses varies from -0.8 to 0 (SD = 0.5), step 0.01. Each value is calculated from 50 times independent random connective and assignment patterns, during 10000 sampling units, under each fixed parameters set. **(b)** The value of synchronization factor of membrane potential for excitatory neurons in the neuron cluster, under mean inhibitory weight of -0.5 in different inhibitory neuron distribution. **(c)** Total membrane potential and typical spike patterns of excitatory neurons with the rebounded synchronization factor curve, in four stages ①-④. In/Ex: inhibitory/excitatory.

spike histogram show that a responsive unit in the VPA suppressed its firing and an excitation rebound later (Rebound type 1 and type 2). The unit without rebound was plotted which exhibited increased firing changes (Non-rebound). The non-responsive unit did not show here. **(b)** The ratio of rebound excitation neural activity by VPA at the left panel and the percentage of type 1 or 2 of the rebound units at the right panel. **(c)** A representative unit with rebound excitation was separated to 4 stages (separated to s1, s2, s3 and s4 by line) based on Figure 1.C. The correlation of rebound units' spikes with the LFP after the VPA injection (Two-tailed unpaired *t* test, ****$p < 0.0001$). **(d)** Representative LFP traces recorded at different time points after VPA injection in KA-induced seizure mice (left: before giving VPA; right: after giving VPA). **(e)** The power spectral density of different frequency range during baseline recording, after KA injection and after VPA injection (left: 3-5 Hz, middle: 6-12 Hz, right: 13-30 Hz, Repeated measures One-way ANOVA, ***$p < 0.001$). **(f)** The coherence of the LFP before and after the VPA injection displayed in different frequency range (left: 3-5 Hz, middle: 6-12 Hz, right: 13-30 Hz, Two-tailed paired *t* test, *$p < 0.05$, ****$p < 0.0001$).

tumors who have not had a seizure, tapering and discontinuing anticonvulsants after the first postoperative week is appropriate".[23] Patients with a preoperative seizure history may be at a higher risk for postoperative seizures following an awake craniotomy.[24] Previous study also revealed that tumor histology, location, intraoperative cortical stimulation, and extent of resection were associated with the occurrence of perioperative seizures.[13] However, a level U evidence indicates tumor location, histology, grade, molecular/imaging features are insufficient when deciding whether or not to prescribe prophylactic ASMs.[25] According to our findings, significant excitatory rebound induced by VPA is an independent factor related to inadequate control of postoperative seizures, but still needs further investigation.

VPA induced excitatory rebound may be related to interictal epileptiform discharges (IEDs). There are mutually exclusive studies have demonstrated that IEDs can be either seizure preventing or seizure facilitating.[26,27] In epilepsy patients, although some antiepileptic drugs can strengthen GABAergic synapses and inhibit neuronal over-excitation, drug resistance is a common problem.[28] As the mechanism of IEDs to seizures is unclear, ASMs may or may not contribute to the transition. According to our findings, the drug resistance may be caused by the generally rebound effect of increasing inhibitory power, which even may contribute to the seizure transition. To elucidate this mechanism, a feasible approach is to recognize the LFP spectrum shift from higher to lower frequency at high amplitude oscillation. In such cases, clinicians should increase the amount of ASMs to cross over the rebound stage before two or three-drug regimens or surgical treatment.

Although the simulation experiment was not very precise, the results partially confirmed excitatory rebound may be an intrinsic character of network dynamics, even in the non-epileptic patients.

Computational models are particularly valuable in the study of epilepsy, which provides a suitable framework for experimental findings, to develop new hypotheses, and to guide future experiments. To describe the complicated dynamics in epilepsy, various theoretical models have been created to study different spatial scales of a system from single channels or receptors to neuron populations and brain regions. Based on the experimental data, detailed models such as multiple neurons with various ion conductance, synapses, and connections have been developed for decades.[29–31] The association between the phenomenological and a network model helps gain a deeper understanding of the robustness of the clinical features among patients. Hodgkin–Huxley equations have many parameters and degrees of freedom,[32] so much more concern was regarded to complicated neuron parameter choices. Here, we chose the intermediate Hindmarsh–Rose neuron models to balance neuron parameters and coupling dynamics. In a recent simulation study using a similar model, inhibitory neurons were demonstrated to contribute to spike waves, including interictal spikes in epileptiform activity, which met the *in vivo* recordings.[33] These simplified neuron models could extract the properties of excitation and inhibition from the electrochemical properties.[11] As the proportion of excitatory/inhibitory neurons was adjusted by various simulations, the rebound phenomenon was universal by the increasing inhibitory power. In addition, the standard deviation of the synchronization factor increased in the rebound band, indicating the probabilistic nature of IEDs to seizures during this period.

To better understand the mechanism underlying refractory epilepsy, we used the KA-induced epilepsy model of mice to investigate the neurophysiological properties of neuronal activities. KA is an agonist that activates the glutamate receptor.[34] VPA exhibits antiepileptogenic effects.[35,36] In our study, the data of behavior and *in vivo* studies showed that the animals had a significant epileptic seizure after KA injection and the seizure was inhibited by VPA injection. Interestingly, there was a significant rebound excitation phenomenon for a long time after drug delivery. Evidence indicates that several receptors such as neurotransmitters increased, and others were involved in hyperexcitability in KA-inducing epilepsy.[37,38] As GABA-ergic interneurons play an important role in the generation of seizures by regulating excitatory-inhibitory balance in the hippocampus, degeneration of GABA-ergic interneurons would be prevented by VPA in the dentate gyrus during drug-induced status epilepticus.[39] Increasing the ratio of inhibitory power in excitatory-inhibitory balance could be the reason for the rebound excitation after VPA treatment.

This study has some limitations. In the context of epilepsy, the functional properties of the neuron cluster model mainly focused on the dynamic of membrane potential and neuron interactions, which are disrupted by a possibly large set of factors at the cellular and molecular levels. Therefore, some biological accuracy to model seizure dynamics is lost in favor of the inhibitory power. The KA-induced animal model is not suitable for all situations, especially for focal seizures. Verification of these results in other epileptic models is required. In human studies, we cannot confirm the incomplete efficacy of valproate until the maximum tolerated dose of the drug is used. Also, VPA dose should be individualized and plasma concentration should be monitored in further study. Although patients were assessed by the OAA/S score, the residual activity from sedative drugs could not be eliminated. In this study, we enroll not only glioma but also cerebral vascular diseases, we believe that our results will be representative in awake craniotomy procedures. Even so, the conclusion drawn from relatively smaller sample size still needs to be further verified.

To summarize, we provide evidence that inadequate control of seizures by VPA monotherapy may be associated with neural excitatory rebound, as predicted by intraoperative ECoG analysis. Combining the shreds of evidence from computational models and animal research, our findings suggest a possible mechanism of inefficient of ASMs that may be because of the excitatory rebound mediated by inhibitory power-induced neuron synchronization and LFP frequency spectrum shift, based on a network intrinsic dynamic mechanism. Based on the current findings, we could choose individual prophylactic ASMs to prevent status epilepticus after awake craniotomy. In future clinical practice, intraoperative ECoG could be broadly applied to guide postoperative anti-seizures regimen, which provides new insight into precision medicine.

Contributors

XZ, YM, LC and DW conceived the project and designed the experiments. XZ, ZZ, YL, ZC, SJ, YT, and ZW did the clinical and animal experiments and analyzed the datasets. YG and HZ built the computational model and did the statistical analysis together with XZ and DW. XZ, ZK, and DW verified the underlying data. XZ, YM, LC and DW wrote the manuscript. All authors critically reviewed the final manuscript. XZ, ZZ, YG and HZ contributed equally to this work. XZ, ZZ have accessed and verified the data, and YM, LC and DW were responsible for the decision to submit the manuscript.

Data sharing statement

The data supporting the findings of this study are available from Dr. WANG (wangdeheng@shutcm.edu.cn) upon request.

Declaration of interests

The authors declare no competing financial interests.

Acknowledgments

We are indebted to epilepsy patients and their relatives for their generous assistance with our research. This work was supported by National Natural Science Foundation of China (62127810, 81970418), Shanghai Municipal Science and Technology Major Project (2018SHZDZX03) and ZJLab; Science and Technology Commission of Shanghai Municipality (18JC1410403, 19411969000, 19ZR1477700, 20Z11900100); MOE Frontiers Center for Brain Science; Shanghai Key Laboratory of Health Identification and Assessment (21DZ2271000); Shanghai Shenkang (SHDC2020CR3073B).

Supplementary materials

Supplementary material associated with this article can be found in the online version at doi:10.1016/j.ebiom.2022.104218.

References

1 Paz JT, Huguenard JR. Microcircuits and their interactions in epilepsy: is the focus out of focus? *Nat Neurosci*. 2015;18(3):351–359.
2 Romoli M, Mazzocchetti P, D'Alonzo R, et al. Valproic acid and epilepsy: from molecular mechanisms to clinical evidences. *Curr Neuropharmacol*. 2019;17(10):926–946.
3 Rogawski MA, Loscher W. The neurobiology of antiepileptic drugs. *Nat Rev Neurosci*. 2004;5(7):553–564.
4 Cunningham MO, Woodhall GL, Jones RSG. Valproate modifies spontaneous excitation and inhibition at cortical synapses in vitro. *Neuropharmacology*. 2003;45(7):907–917.
5 Loscher W. Critical review of current animal models of seizures and epilepsy used in the discovery and development of new antiepileptic drugs. *Seizure-Eur J Epilep*. 2011;20(5):359–368.
6 Beydoun A, Sackellares JC, Shu V, et al. Safety and efficacy of divalproex sodium monotherapy in partial epilepsy: a double-blind, concentration-response design clinical trial. *Neurology*. 1997;48(1):182–188.
7 Striano P, Belcastro V. Treatment of myoclonic seizures. *Expert Rev Neurother*. 2012;12(12):1411–1418.
8 Buechler RD, Buchhalter JR. Juvenile absence epilepsy exacerbated by valproic acid. *Pediatr Neurol*. 2007;36(2):121–124.
9 Belcastro V, Caraballo RH, Romeo A, Striano P. Early-onset absence epilepsy aggravated by valproic acid: a video-EEG report. *Epileptic Disord*. 2013;15(4):440–443.
10 Joiner EF, Youngerman BE, Hudson TS, et al. Effectiveness of perioperative antiepileptic drug prophylaxis for early and late seizures following oncologic neurosurgery: a meta-analysis. *J Neurosurg*. 2018;130(4):1274–1282.
11 Hindmarsh JL, Rose RM. A model of neuronal bursting using three coupled first order differential equations. *Proc R Soc Lond B*. 1984;221(1222):87–102.
12 Marson A, Jacoby A, Johnson A, et al. Immediate versus deferred antiepileptic drug treatment for early epilepsy and single seizures: a randomised controlled trial. *Lancet*. 2005;365(9476):2007–2013.
13 Oushy S, Sillau SH, Ney DE, et al. New-onset seizure during and after brain tumor excision: a risk assessment analysis. *J Neurosurg*. 2018;128(6):1713–1718.
14 Chandran KSS, Mishra A, Shirhatti V, Ray S. Comparison of matching pursuit algorithm with other signal processing techniques for computation of the time-frequency power spectrum of brain signals. *J Neurosci*. 2016;36(12):3399–3408.
15 Kitano Y, Komiyama C, Makino M, et al. Anticonvulsant and neuroprotective effects of the novel nootropic agent nefiracetam on kainic acid-induced seizures in rats. *Brain Res*. 2005;1057(1-2):168–176.
16 Kay HY, Greene DL, Kang S, Kosenko A, Hoshi N. M-current preservation contributes to anticonvulsant effects of valproic acid. *J Clin Invest*. 2015;125(10):3904–3914.
17 Charan J, Kantharia ND. How to calculate sample size in animal studies? *J Pharmacol Pharmacother*. 2013;4(4):303–306.
18 de Araujo Furtado M, Lumley LA, Robison C, Tong LC, Lichtenstein S, Yourick DL. Spontaneous recurrent seizures after status epilepticus induced by Soman in Sprague-Dawley rats. *Epilepsia*. 2010;51(8):1503–1510.
19 Pellock JM, Smith MC, Cloyd JC, Uthman B, Wilder BJ. Extended-release formulations: simplifying strategies in the management of antiepileptic drug therapy. *Epilepsy Behav*. 2004;5(3):301–307.
20 Sommerville KW, Dutta S, Biton V, Zhang Y, Cloyd JC, Uthman B. Bioavailability of a divalproex extended-release formulation versus the conventional divalproex formulation in adult patients receiving enzyme-inducing antiepileptic drugs. *Clin Drug Investig*. 2003;23(10):661–670.
21 Song D, Wang D, Yang Q, et al. The lateralization of left hippocampal CA3 during the retrieval of spatial working memory. *Nat Commun*. 2020;11(1):2901.
22 Liu J, Lyu C, Li M, Liu T, Song S, Tsien JZ. Neural coding of appetitive food experiences in the amygdala. *Neurobiol Learn Mem*. 2018;155:261–275.

23 Glantz MJ, Cole BF, Forsyth PA, et al. Practice parameter: anticonvulsant prophylaxis in patients with newly diagnosed brain tumors. Report of the Quality Standards Subcommittee of the American Academy of Neurology. *Neurology*.. 2000;54(10):1886–1893.

24 Eseonu CI, Eguia F, Garcia O, Kaplan PW, Quinones-Hinojosa A. Comparative analysis of monotherapy versus duotherapy antiseizure drug management for postoperative seizure control in patients undergoing an awake craniotomy. *J Neurosurg*. 2018;128 (6):1661–1667.

25 Walbert T, Harrison RA, Schiff D, et al. SNO and EANO practice guideline update: Anticonvulsant prophylaxis in patients with newly diagnosed brain tumors. *Neuro Oncol*. 2021;23(11):1835–1844.

26 Avoli M, de Curtis M, Kohling R. Does interictal synchronization influence ictogenesis? *Neuropharmacology*. 2013;69:37–44.

27 Karoly PJ, Freestone DR, Boston R, et al. Interictal spikes and epileptic seizures: their relationship and underlying rhythmicity. *Brain*. 2016;139(Pt 4):1066–1078.

28 Schmidt D, Loscher W. Drug resistance in epilepsy: putative neurobiologic and clinical mechanisms. *Epilepsia*. 2005;46(6):858–877.

29 Destexhe A. Can GABAA conductances explain the fast oscillation frequency of absence seizures in rodents? *Eur J Neurosci*. 1999;11 (6):2175–2181.

30 Lytton WW, Omurtag A. Tonic-clonic transitions in computer simulation. *J Clin Neurophysiol*. 2007;24(2):175–181.

31 Zou X, Jiang C, Sun Y, et al. A functional assembly framework based on implementable neurobionic material. *Clin Transl Med*. 2021;11(1):e277.

32 Hodgkin AL, Huxley AF. A quantitative description of membrane current and its application to conduction and excitation in nerve. *J Physiol*. 1952;117(4):500–544.

33 Naze S, Bernard C, Jirsa V. Computational modeling of seizure dynamics using coupled neuronal networks: factors shaping epileptiform activity. *PLoS Comput Biol*. 2015;11(5):e1004209.

34 Tremblay E, Ben-Ari Y. Usefulness of parenteral kainic acid as a model of temporal lobe epilepsy. *Rev Electroencephalogr Neurophysiol Clin*. 1984;14(3):241–246.

35 Mattson RH, Cramer JA, Collins JF. A comparison of valproate with carbamazepine for the treatment of complex partial seizures and secondarily generalized tonic-clonic seizures in adults. The Department of Veterans Affairs Epilepsy Cooperative Study No. 264 Group. *N Engl J Med*. 1992;327(11):765–771.

36 Wang W, Wu J, Li S, et al. Sodium valproate for epilepsy in rural China: an efficacy and safety assessment in primary care. *Epilepsy Res*. 2012;102(3):201–205.

37 Alves M, Gomez-Villafuertes R, Delanty N, et al. Expression and function of the metabotropic purinergic P2Y receptor family in experimental seizure models and patients with drug-refractory epilepsy. *Epilepsia*. 2017;58(9):1603–1614.

38 Soares JI, Valente MC, Andrade PA, Maia GH, Lukoyanov NV. Reorganization of the septohippocampal cholinergic fiber system in experimental epilepsy. *J Comp Neurol*. 2017;525(12):2690–2705.

39 Wei D, Yang F, Wang Y. Degeneration and regeneration of GABAergic interneurons in the dentate gyrus of adult mice in experimental models of epilepsy. *CNS Neurosci Ther*. 2015;21 (1):52–60.